

Large-scale atomistic simulations demonstrate dominant alloy disorder effects in $\text{GaBi}_x\text{As}_{1-x}/\text{GaAs}$ multiple quantum wells

Muhammad Usman^{1,*}

¹*School of Physics, The University of Melbourne,
Parkville, Melbourne, 3010, Victoria Australia.*

Abstract

Bismide semiconductor materials and heterostructures are considered a promising candidate for a wide range of photonic, thermoelectric, photovoltaic, and spintronic devices. This work presents a comprehensive theoretical study of the electronic and optical properties of strongly-coupled $\text{GaBi}_x\text{As}_{1-x}/\text{GaAs}$ multiple quantum well (QW) structures based on a systematic set of large-scale atomistic tight-binding calculations. Our results reveal that atomic-level fluctuations in alloy compositions overcome the coupling effects and dictates the overall QW properties. Independent of QW geometry parameters, the alloy disorder leads to a strong confinement of charge carriers, a large broadening of the hole energies, and a red shift in the ground-state transition wavelengths. Polarisation-resolved optical transition strengths exhibit a striking effect of disorder, where the inhomogeneous broadening could exceed an order of magnitude for multiple QWs, in comparison to a factor of three for single QWs. The dominance of alloy disorder effects persists in the presence of experimental uncertainties in the size and composition of QWs. The presented results highlight the limitations of continuum methods and emphasise on the need of large-scale atomistic approaches for designing of devices with tailored functionalities based on the novel properties of bismide materials.

1. INTRODUCTION

Bismide alloys formed by dilute impurity concentrations of Bi atoms in GaAs are a rapidly emerging material system for the design of photonic devices [1–4], photovoltaics [5–7], spintronic devices [8], and thermoelectric applications [9]. The experimental and theoretical investigations of both unstrained and strained bulk $\text{GaBi}_x\text{As}_{1-x}$ alloys have shown promising properties with increasing Bi fractions such as a large band gap reduction [10, 11], a crossover between the band gap and spin split-off energies [11, 12], and the possibility of lattice-matched growth on GaAs substrates [13]. These novel characteristics have sparked a remarkable experimental interest in designing devices based on $\text{GaBi}_x\text{As}_{1-x}/\text{GaAs}$ quantum well (QW) structures which could offer optimised performance [2, 14–20]. To fully exploit the benefits of Bismide QWs for a desired device operation, one open question is to understand the impact of fluctuations in the spatial positions of Bi atoms (also known as alloy disorder) on the electronic and optical properties of multiple quantum well (MQW) structures. In particular, it is yet unknown how the interplay between alloy disorder, inter-well couplings and geometry parameters will determine the overall device performance. This letter, based on large scale atomistic simulations, provides key insights on the role of alloy disorder in $\text{GaBi}_x\text{As}_{1-x}/\text{GaAs}$ MQW structures and the established knowledge will pave the way for the design of future devices with tailored functionalities.

Despite significant ongoing experimental efforts [2, 14–20] on $\text{GaBi}_x\text{As}_{1-x}/\text{GaAs}$ MQW structures and superlattices, the existing literature lacks theoretical guidance on the understanding and design of these nano-structures. We investigate the impact of alloy disorder by performing a systematic set of simulations. We first start with hypothetical ordered QW devices, which contains ordered (uniform) distribution of Bi atoms such as illustrated in Fig. 1 (a). In the absence of disorder, the electronic properties of these devices are dictated by inter-well couplings. The confined charge carriers form strongly coupled molecular states as evident from electron and hole charge density plots shown in Fig. 1 (b). By increasing number of QWs from one to four and also by increasing the separation between QWs from 2 nm to 16 nm, we thoroughly study the evolution of electronic states governed by the underpinning coupling effects. Next, we *switch on* disorder in the QW regions by randomly placing the same fraction of Bi atoms as depicted in Fig. 1 (c). Keeping all other geometry parameters unchanged, a direct comparison with the ordered case unravels the strong impact of alloy disorder, which overcomes the coupling effect and dictates the confinement of charge carriers (Fig. 1 (d)). During the growth of QW devices, small uncertainties in the geometry parameters are inevitable, therefore we also study ± 1 nm variation in QW width

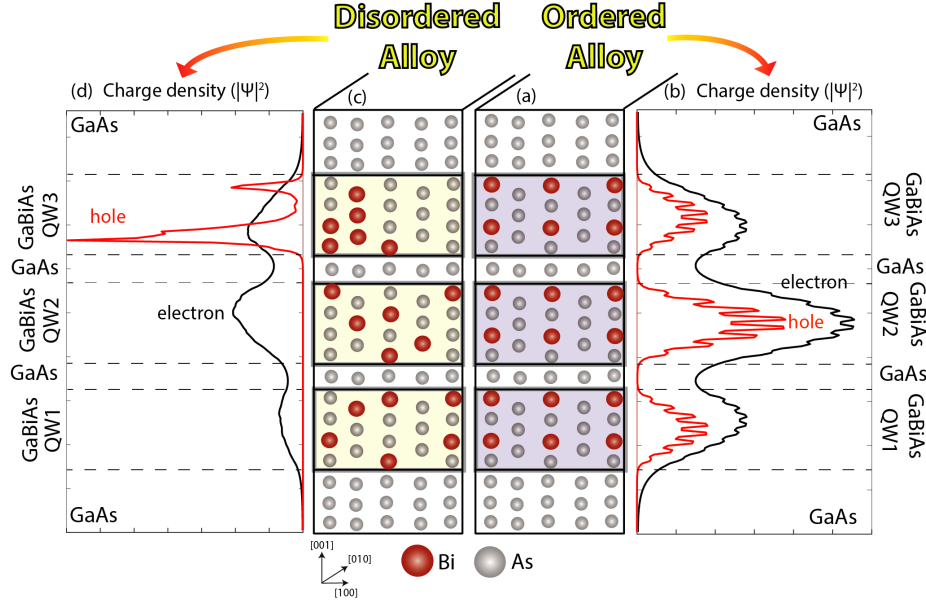


FIG. 1. **Ordered vs. disordered multiple quantum wells:** Schematic diagrams of two quantum well structures are shown in (a) and (b). Both structures consists of three $\text{GaBi}_x\text{As}_{1-x}$ quantum wells, separated by GaAs spacer layers. All geometry parameters and Bi compositions are identical, except the spatial distribution of Bi atoms in the QW regions. The structure in (a) exhibits uniform distribution of Bi atoms (ordered alloy), whereas the one in (b) has Bi atoms randomly distributed in the QW regions (disordered alloy). The impact of fluctuations in Bi atom positions is clearly evident in the electron and hole charge density plots shown in (c) and (d). Ordered structure shows strongly coupled charge carrier states, whereas disorder overcomes the inter-well coupling effect leading to much stronger confinement of charge carriers (in particular hole) due to the formation of Bi pairs and clusters.

and 0.5% change in Bi composition. Our results indicate the dominant role of alloy disorder in spite of these fluctuations in the geometry parameters, confirming that the disorder related effects would control the electronic and optical properties of MQW structures under realistic experimental environments.

It would be worth highlighting here that the study of alloy disorder is particularly a challenging problem because it requires theoretical modelling of $\text{GaBi}_x\text{As}_{1-x}/\text{GaAs}$ QW structures with atomistic resolution and the simulation need to be performed over a large size of supercell [12, 21]. Majority of the existing literature on bulk $\text{GaBi}_x\text{As}_{1-x}$ materials either rely on the simplified envelope wave function approximations such as effective-mass or $k \cdot p$ [2, 22] which ignore the alloy fluctuations, or based on DFT simulations [23, 24] which are restricted to smaller size of supercells. This work overcomes both challenges by establishing an atomistic tight-binding framework

which can simulate realistic $\text{GaBi}_x\text{As}_{1-x}$ QWs with random placement of Bi atoms. Furthermore, the simulation domains consist of several thousands atoms, capturing the true nature of disorder related effects.

2. METHODS

Geometry of QW Devices and Methods: In our calculations, a QW device is defined by four parameters: the width (w) of QW region along the (001) direction, the separation (d) between the adjacent QWs, total number (n) of QWs in the device, and the Bi composition (x) of a QW. To study the effects of inter-well coupling and disorder, we fix $x=3.125\%$ and $w=8$ nm, and investigate the variation in $n \in \{1, 2, 3, 4\}$ and $d \in \{2, 4, 6, 8, 12, 16\}$ nm. In the last part of this work, we introduce small changes in x and w to probe the strength of disorder effects in the presence of small variations in geometry parameters. The simulation domain consists of 16 nm of GaAs substrate and capping layer, and the lateral dimensions are 4 nm which have been shown as large enough to realistically capture the alloy disorder effects [12]. The boundary conditions are periodic in all three dimensions. A single QW region consists of 4096 atoms (out of which 128 are Bi atoms) and the largest QW structure corresponding to $n=4$ and $d=16$ nm consists of 114,688 atoms in the simulation domain. Further details about the geometry parameters are provided in *supplementary section S1*.

The atoms are relaxed using a valence force field (VFF) model [11, 25], and hydrostatic (ϵ_H) and biaxial (ϵ_B) strain components are computed from the relaxed atom positions (see *supplementary section S2* for details). The electronic structure is calculated by solving ten-band sp^3s^* tight-binding Hamiltonian including spin-orbital coupling [11]. The polarisation resolved transverse electric (TE) and magnetic (TM) inter-band optical transition strengths are computed from Fermi's golden rule by evaluating momentum matrix elements between the ground electron and hole states. Full details of the electronic and optical methods are provided in the *supplementary section S3*.

3. RESULTS AND DISCUSSIONS

Effect of inter-well coupling in ordered QWs: To investigate the inter-well coupling effect, we first artificially switch off alloy disorder by uniformly placing 128 Bi atoms in the QW regions (one Bi atom per four unit cells of GaAs). Fig. 2 (a-d) plots the strain profiles for the ordered QW devices along the (001) axis through the centre of QWs for $n=1, 2, 3$, and 4 respectively

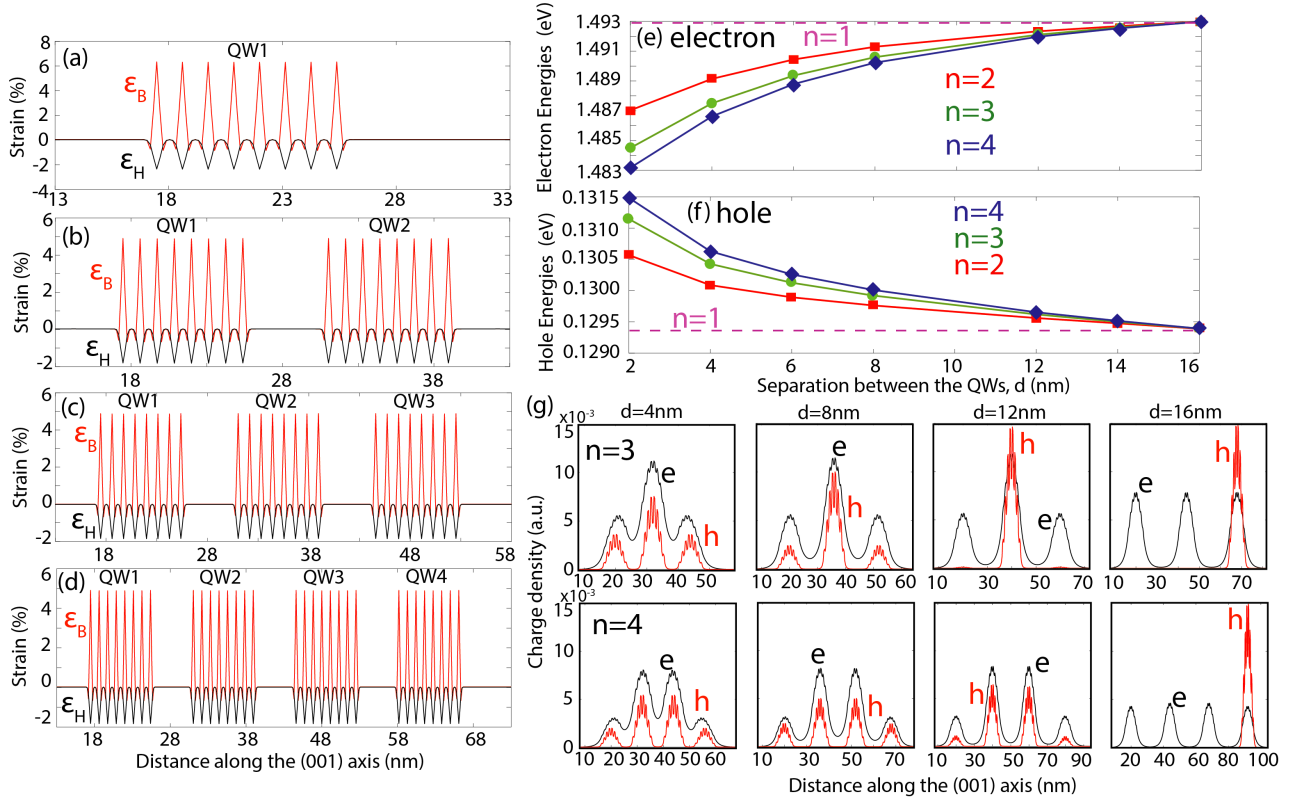


FIG. 2. **Inter-well coupling effects in ordered MQW devices:** (a-d) The line plots of hydrostatic (ϵ_H) and biaxial (ϵ_B) strain components as a function of distance along the (001) axis are shown through the centre of QWs for $n=1, 2, 3$, and 4 . The separation d between the QWs is 4 nm and the widths of QWs are 8 nm. (e, f) Plot of the lowest electron and the highest hole energy levels are shown as a function of the separation (d) between the QWs for $n=2, 3$, and 4 . The horizontal dashed lines indicate energy levels for a single QW device. (g) Plots of the lowest electron and the highest hole state charge densities as a function of distance along the (001) axis are shown for a few selected separations d and for $n=3$ and 4 .

and $d=4$ nm. The peaks indicate the accumulation of strain in the vicinity of Bi atoms. The positive (negative) sign of ϵ_B (ϵ_H) is due to larger lattice constant of GaBi in comparison with GaAs, which is consistent with existing studies on other III-V heterostructures [26]. Overall we find that there is a small change in the strain parameters when the number of QWs are increased.

Fig. 2 (e) and (f) plots the lowest electron and the highest hole energies as a function of QW separation for $n=1, 2, 3$, and 4 . As the separation between the QWs is reduced, strong inter-well coupling leads to decrease (increase) in the electron (hole) energies. To further study the strength of inter-well couplings as a function of d , we also plot line-cut profile of electron and hole

charge (or probability) densities (computed by *equations 6 and 7 in supplementary material*) as a function of distance along the (001) axis for a few selected inter-well separations. Fig. 2 (g) shows charge density plots for $n=3$ and 4, and the plots for $n=1$ and 2 are provided in the *supplementary sections S4 and S5*. The strong inter-well coupling leads to hybridized bonding-like electron and hole states for small inter-well separations ($d=4$ and 8 nm). The coupling becomes weak for $d=12$ and 16 nm, in particular the hole states are found to be completely decoupled at 16 nm separation and are confined in a single QW region. The electron states on the other hand experience lesser confinement effect, and therefore become decoupled at 24 nm separation. The overall shape and confinement of the electron and hole ground states for the ordered QW devices is consistent with what we expect from the envelope wave function approximation approach.

Disorder effects in realistic MQW structures: In realistic QW devices, fluctuations in the distribution of Bi atoms inside the $\text{GaBi}_x\text{As}_{1-x}$ QW regions are expected and recent experiments have shown the evidence of clustering of Bi atoms [27, 28]. Therefore it is crucial to investigate the effects of disorder to properly understand the experimental measurements and to design device with desired functions. Here we study the effect of alloy disorder by randomly placing 128 Bi atoms ($x=3.125\%$) in each QW region of a MQW structure. To properly model the disorder in Bi atom positions and to quantify the related inhomogeneous broadening of electron and hole energies, we consider five different random placements for Bi atoms. Fig. 3 (a-d) plots the strain profiles for one particular exemplary random distribution of Bi atoms, and for $d=4$ nm and $n=1, 2, 3$, and 4 (the plots for other Bi configurations exhibit similar profile). The distribution of strain peaks is arbitrary due to the random occurrence of Bi atoms at the As positions and clearly imitate the disordered character. Notably compared to the strain profiles for the ordered cases, the overall magnitude of the strain components have been reduced by approximately a factor of two. This is because for ordered case, each Bi atom is connected to four neighbouring As atoms and therefore exhibit sharp peaks in the strain profiles. However the disordered alloy is a mixed configuration of Bi atoms, with some of them being closer to each other, and therefore the strain profiles show smaller peaks but more distributed nature.

Fig. 3 (e) and (f) plots the lowest electron and the highest hole energies as a function of the QW separations d for $n=1, 2, 3$, and 4. Both electron and hole energies are broadened due to alloy disorder, though the broadening of electron energies is quite small (of the order of 1 to 2 meV), which is nearly independent of n and d . The hole energies are significantly affected by the presence of alloy disorder and show a large broadening. The broadening of hole energies is further

highlighted in *supplementary Fig. S4* for $n=1, 2, 3$, and 4 devices. Our results indicate that for the single QW device the broadening is 31 meV, which varies over a wide range (from 4 meV to 64 meV) for MQW structures ($n > 1$). On average, we predict that a broadening of 10-40 meV is expected for coupled QW devices. The stronger disorder effect on hole energies compared to the electron energies is also expected because the Bi related resonant states are predicted to lie closer to the valence band edge of GaAs, and therefore a large band-anticrossing type interaction between the valence bands will induce a correspondingly large disorder related effects on the hole states [11, 21].

In terms of electron and hole energy shifts, we find that the dependence of electron energies on d is quite similar to what we expect for strongly coupled ordered QWs (decrease in energy when d is reduced), which again indicates that the disorder related effects are relatively weak for electron states. When the number of QWs are increased from 1 to 4, the decrease in electron energy is around 10 meV which is same as observed earlier for ordered QW devices (Fig. 2 (e)). Disorder further increases the electron energies by about 1 meV. The hole energies on the other hand show large variations irrespective of d and n , and exhibit no coupling effect. Therefore we cannot characterize the change in the hole energies as increase or decrease as a function of d . The introduction of alloy disorder however causes a large upward shift of about 60 meV in the hole energies. Therefore we predict an overall red shift in the ground state transition energies due to the alloy disorder in the MQW structures.

Although the variation in electron and hole energies provides some understanding of the impact of disorder, the electron and hole charge density plots exhibit much clearer picture of the overall electronic characteristics of QW devices. Fig. 3 (g) shows the charge density plots for a few selected values of d and n and one particular random distribution of Bi atoms. Plots for other values of n and three random distributions of Bi atoms are provided in the *supplementary section S6*. For reference, we also provide plots for single QW devices in *supplementary Fig. S2*. The plots for single QWs show that while the hole states are significantly perturbed (much more confined), the electron states largely retain their envelope wave function approximation type character. Strikingly for the coupled QW systems, we find that the electron states are also significantly perturbed and for some cases, their confinement is much stronger than what we expect from coupling effects only. For example, in *supplementary Fig. S6* the confinement of the electron states for $d=6$ nm and $n=3$ is entirely in the upper two QW regions (for all three random distributions of Bi atoms) indicating the breakdown of coupling effect. It is not possible to capture such character in simple theoretical

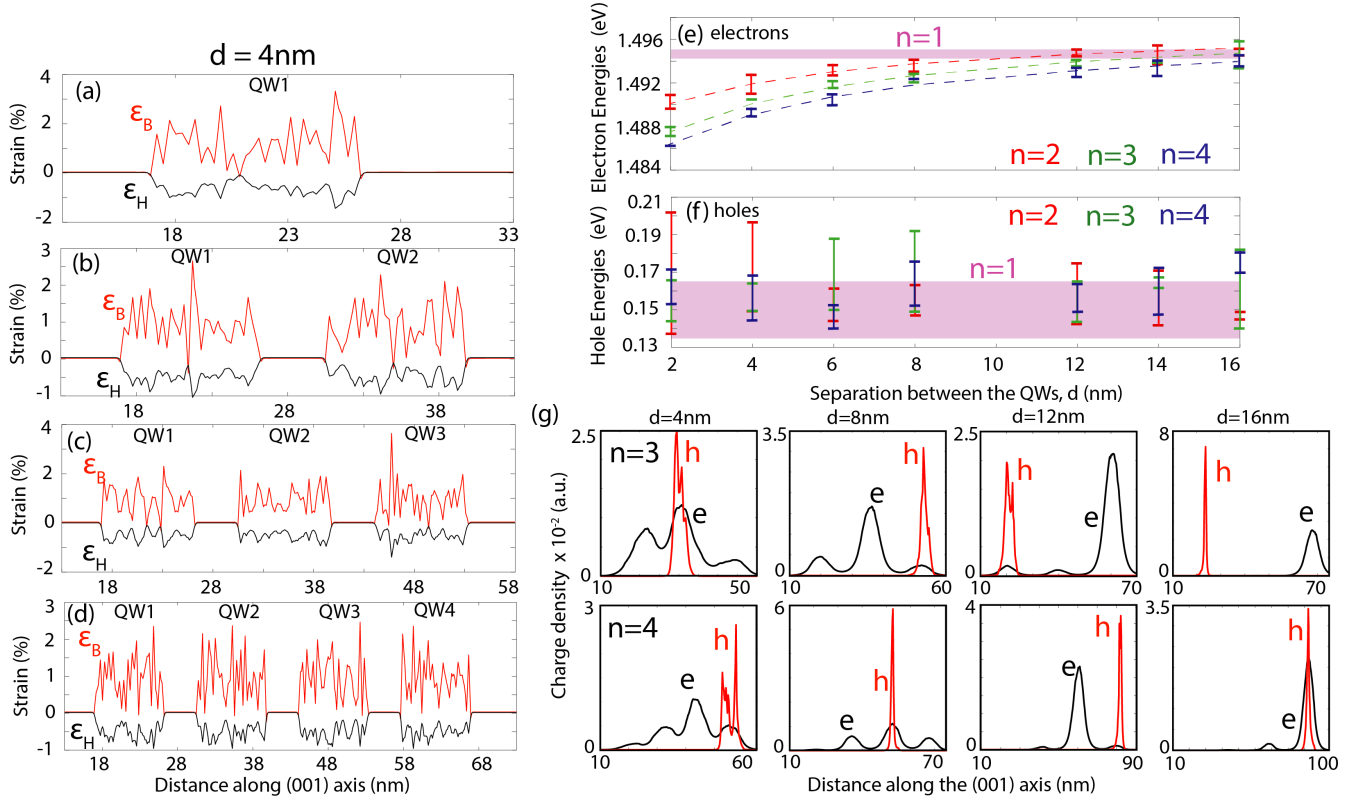


FIG. 3. **Dominant role of alloy disorder in MQW structures:** (a-d) The line plots of hydrostatic (ϵ_H) and biaxial (ϵ_B) strain components as a function of distance along the (001) axis are shown through the centre of QWs for $n=1, 2, 3$, and 4 . The separation between the QWs is 4 nm and the widths of QWs are 8 nm. (e, f) Plots of the lowest electron and the highest hole energy levels are shown as a function of the separation (d) between the QWs for $n=2, 3$, and 4 . The error bars show the broadening of energies computed over five different random distributions of Bi atoms in the QW regions. The dashed lines in (e) are plotted as a guide to eye to indicate the overall trend of variation in electron energies. The shaded areas indicate energy level broadening for a single QW ($n=1$). (g) Plots of the lowest electron and the highest hole state charge densities as a function of distance along the (001) axis plotted are shown for a few selected separations d and for $n=3$ and 4 .

models such as effective-mass or k·p which ignore disorder. Another consequence of alloy disorder on electron states is evident from plots for $d=16$ nm cases, where the electron states show single QW confinements in contrast to the ordered case where such confinement is possible at much larger values of d . Therefore we show that the existing notion, based on bulk alloy studies and single QW structures, that the alloy disorder negligibly impacts the probability density of conduction band states cannot be applied to MQW structures.

The hole states do not exhibit any coupling effect in the presence of disorder and are always strongly confined in a single QW region for MQW structures. Moreover, the presence of hole states in a particular QW region is entirely arbitrary and is very sensitive to the strength of disorder (the presence of pairs and clusters) in that QW region. This arbitrary nature of hole confinements implies that the electron-hole wave function overlap would significantly vary from device to device even with the same geometry parameters: x , n , d , and w . This character is shown in the *supplementary Fig. S8*, where we have plotted electron-hole wave function overlaps as a function of d for $n=2, 3$, and 4 . For reference, we have also included values for the corresponding ordered cases. While the ordered cases show an almost constant value of overlap for small values of d (strongly coupled regime), and a decrease as d becomes large. However, for the disordered cases, not only a significant reduction in the electron-hole wave function overlap is computed due to much stronger confinement of the hole states, but also there is a large variation in the magnitudes of the computed overlaps due to arbitrary nature of the hole positioning inside the QW devices.

Polarisation-resolved optical transitions strengths: The polarisation dependent TE and TM inter-band optical transition strengths are modulated by the following effects: (i) overlap between the electron and hole state, (ii) coupling between the QWs which increases TM mode, and (iii) conventional selection rule which allows transitions between Eigen states of certain character. For compressively strained QWs such as $\text{GaBi}_x\text{As}_{1-x}/\text{GaAs}$, the highest hole state is predicted to have heavy-hole character and therefore TM mode transition is prohibited from the selection rule. Indeed we find zero magnitude of TM mode transition for ordered QW structures. The presence of disorder breaks down the coupling effect and selection rule, allowing some mixing of p_z character in the highest hole state, giving rise to small amplitude of TM mode transition as shown in Fig. 4.

For TE mode transition, its magnitude is strongly dependent on overlap between the electron and hole wave functions. As we have discussed above that the presence of disorder significantly perturbs the electron and hole states, leading to strong confinement of hole states which reduces electron hole wave function overlaps. Moreover the overlap between electron and hole states exhibits large variation. These two effects will not only reduce the overall strength of TE mode, but also induce a large variation in its magnitude. This is shown in Fig. 4 where we plot TE mode strengths as a function of QW separation for $n=2$. Same plots for $n=3$ and 4 are provided in the *supplementary Fig. S9*. For comparison, we also plot corresponding values for ordered cases. Overall a clear reduction in the inter-band transition strengths is observed for disordered structures. Large variations in TE mode are a direct consequence of highly confined hole states

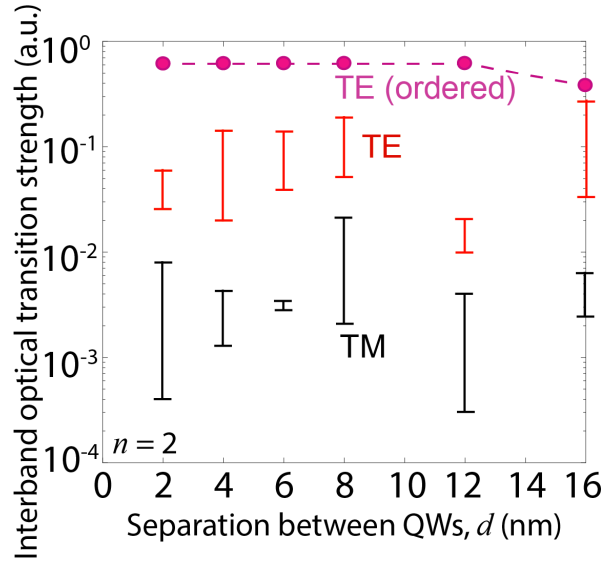


FIG. 4. **Polarisation-resolved inter-band optical transition strengths:** Plots of the polarisation-dependent inter-band optical transition strengths are shown as a function of the distance along the (001) axis for $n=2$. The error bars are for disordered $\text{GaBi}_x\text{As}_{1-x}$ QW structures and indicate the broadening of transition strengths due to fluctuations in Bi atom positions.

which lead to large variations in wave function overlaps. Notably we find that the variation in TE mode are of the order of factor of ten which is significantly higher than the single QW devices where this variation was about a factor of three [21]. This is due to the fact that for single QW device, electron wave function is negligibly perturbed and retains its envelope wave function approximation type character. Moreover both electron and hole state reside in the same QW region, therefore relatively small changes occur in the electron-hole wave function overlap. Contrarily for MQW structures, the stronger confinement of both electron and hole states, in conjunction with arbitrary selection of a QW region for the hole confinement leads to a much larger variation in the inter-band transition strengths.

Interplay between disorder and geometry parameters: From Fig. 3, it is clear that the presence of disorder strongly influences the electronic properties of MQW devices. However in our discussion so far, we have fixed the widths ($w=8$ nm) and Bi compositions ($x=3.125\%$) of QWs. In a realistic experimental environment, these geometry parameters are hard to control and small variations are inevitable. Therefore it is important to investigate alloy disorder effects in the presence of small variations in w and x .

Let's first investigate Bi composition of QWs. For this purpose, we select an exemplary triple

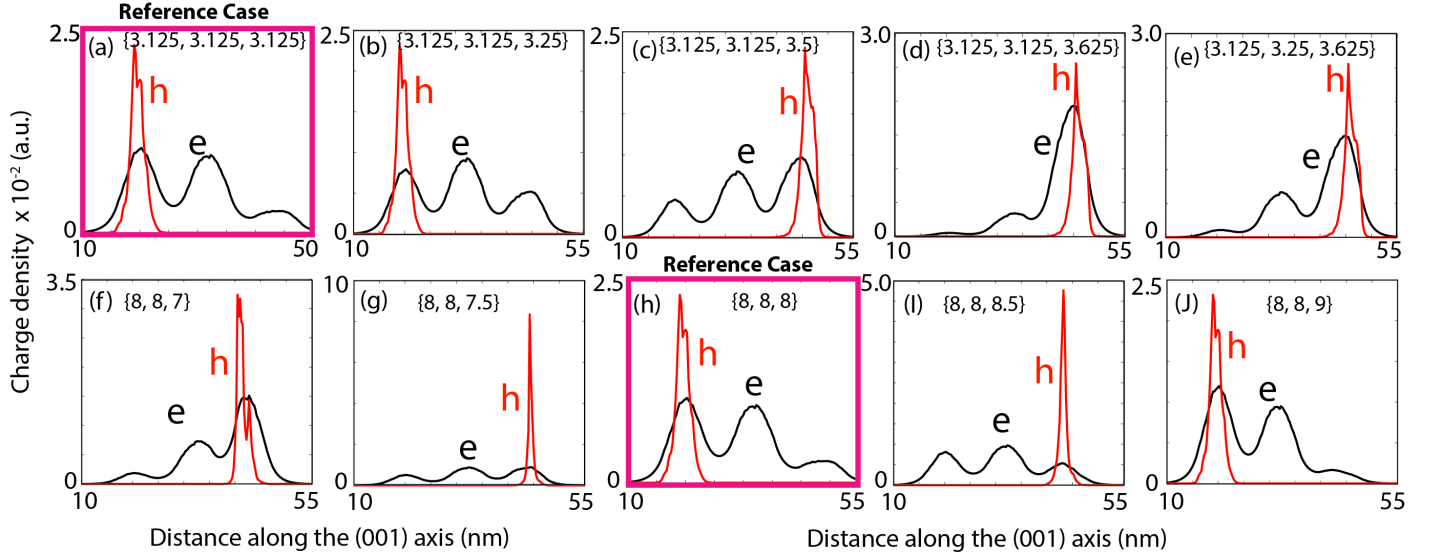


FIG. 5. **Interplay between alloy disorder and geometry parameters:** (a-e) The Bi fraction of a triple QW structure ($n=3$) is varied as indicated by labels $\{x_1, x_2, x_3\}$, where x_1, x_2 , and x_3 are the Bi fractions of the lowest, middle and top QWs, respectively. The widths w of all three QW regions are 8 nm and the separation between the QWs is 4 nm. (f-j) The widths of QWs in a triple QW structure ($n=3$) are varied as indicated by labels $\{w_1, w_2, w_3\}$, where w_1, w_2 , and w_3 are the widths of the lowest, middle and top QWs, respectively. The Bi fraction x of all three QW regions is 3.125% and the separation between the QWs is 4 nm.

QW structure with $d=4$ nm and $w=8$ nm. The Bi compositions of three QWs in this device are represented by $\{x_1, x_2, x_3\}$. Fig. 5 (a) plots the electron and hole charge densities for the reference case where the composition is uniform ($x_1 = x_2 = x_3=3.125\%$). The confinement of hole state in the lowest QW region indicates that the disorder is strongest in this QW region. It is known from the composition dependence of electron and hole energies in bulk $\text{GaBi}_x\text{As}_{1-x}$ alloys that increasing x of a QW will increase (decrease) the valence (conduction) band energies for that particular QW [11], thereby pulling the electron and hole states inside it. In Figs. 5 (b) to (d), we gradually increase the Bi composition of the topmost QW and plot the electron and hole charge densities. The electron charge density gradually moves towards the upper QWs, however the hole charge density remains in the lowest QW until x is increased by 0.25% or more. This shows that the alloy disorder effect is dominant over the Bi composition effect for up to 0.25% variation in x , which is also evident from a second case of quadruple QW structure discussed in *supplementary section S7*. Note that we have chosen the extreme case by increasing x of the topmost QW region. If instead x for the lowest QW is increased, the hole state will stay confined inside it and the

electron state will also increasingly confine in the lowest QW. Similar effect is shown in Fig. 5 (e) where we increase the Bi composition of middle QW compared to part (d). The hole state remains in the upper-most QW indicating dominant disorder effect, but the confinement of electron state slightly increases in the middle QW region.

Next we probe fluctuations in the width of QW by keeping the other parameters fixed at $x=3.125\%$, $d=4$ nm. Fig. 5 (h) shows the reference case where all the three QWs have uniform width of 8 nm. In conventional MQW structures, if the width of a QW region is increased (decreased), it reduces (increases) the confinement energies of charge carriers and therefore the ground electron and hole states will tend to reside in the larger width QW region [29]. However for highly mismatched alloys such as $\text{GaBi}_x\text{As}_{1-x}$, if x is kept fixed, the increase (decrease) in the QW width will lead to weaker (stronger) alloy disorder effect and therefore it will push the electron and hole ground states away from the larger QW region. Therefore changing the width of QW introduces two competing effects (from disorder and change in confinement energies). This interplay between the two competing effects is observed in Figs. 5 (f-j). When the QW width is decreased from 8 nm to 7 nm, both the electron and hole states moves into the smaller width QW indicating alloy disorder effect dominating the QW width effect. On the other hand, for the larger QW width (changing from 8 to 9 nm), at first the geometry effect pushes the hole state towards the wider QW region, but at 9 nm the alloy disorder effect again dominates and leads to electron and hole states being outside of the wider QW.

In *supplementary section S7*, we have discussed fluctuations in x and w for a second case with $n=4$, concluding that the alloy disorder effects overall dominates the impact of QW width variations. Overall we conclude that disorder plays a dominant role in determining electronic and optical properties of MQW devices even in the presence of ± 1 nm variation in w and up to 0.25% variation in the x .

4. CONCLUSIONS

In summary, based on large-scale atomistic tight-binding calculations, we have shown the dominant nature of alloy disorder effects which dictate the electronic and optical properties of $\text{GaBi}_x\text{As}_{1-x}/\text{GaAs}$ MQW devices. The direct comparison of ordered and disordered QW structures provides a quantitative estimate of disorder related inhomogeneous broadening and energy shifts of the electron and hole ground states. We show that the electron states are significantly perturbed by fluctuations in Bi atom positioning, in contrast to existing notion that the conduction

band states are negligibly impacted by disorder. Overall we conclude that disorder related effects are stronger in MQW devices compared to bulk and single QW structures, and their dominant role persist in the presence of small uncertainties in the geometry parameters. The presented results provide critical insights for understanding and designing a wide range of photonic devices, photovoltaics, spintronics, and thermoelectric applications with tailored functionalities based on novel characteristics of Bismide materials.

Acknowledgements: Computational resources are acknowledged from NCN/Nanohub. Some parts of this work were carried out at Tyndall National Institute, Cork Ireland.

Supplementary Material Section

S1. Geometry Parameters of Multiple Quantum Well Structures

Figure S1 shows the schematic diagram of $\text{GaBi}_x\text{As}_{1-x}/\text{GaAs}$ multiple quantum well (MQW) structures studied in this work. A MQW device consists of n number of QWs separated by d nm thick GaAs spacer layers. To investigate the effect of inter-well couplings, we have simulated MQW structures with $n \in \{1, 2, 3, 4\}$ and $d \in \{2, 4, 6, 8, 12, 16\}$ nm. The width w of each QW region is 8 nm. First we have investigated inter-well couplings and alloy disorder effects based on uniform geometry parameters: $w=8$ nm and $x=3.125\%$ for all the QW regions in the MQW device. In the last part of our work, we investigate the interplay between alloy disorder and geometry parameters by introducing ± 1 nm variation in w and 0.5% variation in x .

For the uniform geometry MQW devices, 128 As atoms are replaced by Bi atoms to form $\text{GaBi}_x\text{As}_{1-x}$ QWs with $x=3.125\%$. To study the effect of inter-well couplings, we first switch off disorder in Bi positions and uniformly place 128 Bi atoms in the QW regions. For disordered devices, the placement of Bi atoms is done by randomly selecting 128 As locations out of 4096 possible positions. We perform simulations for five different random configurations of Bi atoms to determine the inhomogeneous broadening of electron and hole energies due to the fluctuations in Bi atom positions.

To investigate the alloy disorder effects in realistic environment, we perform large-scale atomistic

simulations consisting of several thousand atoms in the supercell. The thickness of both GaAs substrate and capping layer is 16 nm along the (001) direction, which is sufficient to allow proper strain relaxation. The size of lateral domain in the (001)-plane is $4 \times 4 \text{ nm}^2$, which has been shown to be large enough for realistically capturing the alloy disorder effects [12, 21]. The overall size of the simulated supercell for the smallest QW device ($d=2 \text{ nm}$, $n=2$, $w=8 \text{ nm}$) is $50 \times 4 \times 4 \text{ nm}^3$ consisting of 51,200 atoms, and for the largest device ($d=16 \text{ nm}$, $n=4$, $w=8 \text{ nm}$) is $112 \times 4 \times 4 \text{ nm}^3$ consisting of 114,688 atoms. The boundary conditions are periodic in all three dimensions.

S2. Calculation of Strain

In order to calculate strain induced by lattice-mismatch between GaAs and $\text{GaBi}_x\text{As}_{1-x}$ materials, the $\text{GaBi}_x\text{As}_{1-x}/\text{GaAs}$ MQW supercells are relaxed by applying atomistic valence force field (VFF) energy minimization scheme [11, 25, 30]. The VFF parameters for GaBi and GaAs materials are provided in ref. [11]. The values of α_0 and β_0 for the GaAs are taken from Lazarenkova *et al.* [30], whereas for GaBi are determined by obtaining relaxed bond lengths in accordance with the Kent *et al.* [31].

After the VFF relaxation, the strain tensor components ($\epsilon_{xx}, \epsilon_{yy}, \epsilon_{zz}, \epsilon_{xy}, \epsilon_{yz}, \epsilon_{xz}$) are computed from the relaxed bond lengths of atoms [30]. The strain parameters of interest which could be directly related to energy shifts in conduction and valence band edges are hydrostatic (ϵ_H) and biaxial (ϵ_B) strains, which are defined as follows [26]:

$$\epsilon_H = \epsilon_{xx} + \epsilon_{yy} + \epsilon_{zz} \quad (\text{S1})$$

$$\epsilon_B = 2\epsilon_{zz} - \epsilon_{xx} + \epsilon_{yy} \quad (\text{S2})$$

It should be noted that for compressively strained heterostructure such as studied in this work, the hydrostatic strain will be negative introducing a reduction in electron energy levels and the biaxial strain will be positive, leading to a net increase in the hole energy levels [26].

S3. Calculation of Electronic Structure and Polarisation Resolved Optical Transition Strengths

The electronic structure of MQW devices is computed from the nearest-neighbour ten-band sp^3s^*

tight-binding theory, which explicitly include spin-orbit coupling. The tight-binding parameters for GaAs and GaBi materials are derived to accurately reproduce the bulk band structure of these materials [11]. By solving the tight-binding Hamiltonian, we obtain ground state electron and hole energies and wave functions, which are labelled as $|\psi_e\rangle$ and $|\psi_h\rangle$, respectively, and defined as:

$$|\psi_e\rangle = \sum_{i,\mu} C_{i,\mu}^e |i\mu\rangle \quad (\text{S3})$$

$$|\psi_h\rangle = \sum_{j,\nu} C_{j,\nu}^h |j\nu\rangle \quad (\text{S4})$$

where the label i (j) represents the atom number inside the supercell and μ (ν) denotes the orbital basis states on an atom for electron (hole) states.

The overlap between the electron and hole ground states is computed as follows:

$$|\langle\psi_h|\psi_e\rangle| = \sum_{i=j} \sum_{\mu=\nu} |(C_{j,\nu}^h)^* C_{i,\mu}^e| \quad (\text{S5})$$

The charge density plots of the electron and hole ground states as a function the distance along (001) or z -axis are computed by average over the probability densities associated with all atom in the plane corresponding to a value at z axis:

$$|\psi_e(z)|^2 = \frac{1}{\text{total \# of atoms at } z} \sum_{\text{all atoms at } z} |\langle\psi_e|\psi_e\rangle|^2 \quad (\text{S6})$$

$$|\psi_h(z)|^2 = \frac{1}{\text{total \# of atoms at } z} \sum_{\text{all atoms at } z} |\langle\psi_h|\psi_h\rangle|^2 \quad (\text{S7})$$

Note that we have only shown charge density plots for anion atom planes. The plots for cation atom planes exhibit similar behaviour [21] and are omitted for simplicity.

The inter-band momentum matrix elements between the ground electron and hole states is computed as follows:

$$M_{\vec{n}}^{\alpha\beta} = \sum_{i,j} \sum_{\mu,\nu} (C_{i,\mu,\alpha}^e)^* (C_{j,\nu,\beta}^h) \langle i\mu\alpha | \mathbf{H} | j\nu\beta \rangle (\vec{n}_i - \vec{n}_j) \quad (\text{S8})$$

where α and β represent spin of states, \mathbf{H} is the sp^3s^* tight-binding Hamiltonian, and $\vec{n} = \vec{n}_i - \vec{n}_j$ is the real space displacement vector between atoms i and j , and is either equal to $\vec{x}_i - \vec{x}_j$ for the TE mode calculation or is equal to $\vec{z}_i - \vec{z}_j$ for the TM mode calculation. The optical transition strengths (TE₁₀₀ and TM₀₀₁) are then calculated by using Fermi's Golden rule and summing the absolute values of the momentum matrix elements over the spin degenerate states:

$$\text{TE}_{100} = \sum_{\alpha,\beta} |M_{\vec{x}}^{\alpha\beta}|^2 \quad (\text{S9})$$

$$\text{TM}_{001} = \sum_{\alpha,\beta} |M_{\vec{z}}^{\alpha\beta}|^2 \quad (\text{S10})$$

The tight-binding model is implemented within the framework of atomistic tool NanoElectronic Modeling (NEMO 3-D) simulator [32, 33] which has, in the past, shown an unprecedented accuracy to match experiments for the study of nano-materials [11, 12, 34] and devices [26, 35].

S5. Charge densities for single quantum well devices

Figure S2 plots the charge densities for single QW devices as a function of the distance along the (001) axis. For a direct comparison, we show both ordered and disordered (three different random configurations of Bi atoms) charge density plots. From the ordered QW simulation, the plots of charge density closely resemble to what we expect from envelope wave function approximation methods. Both electron and hole states are symmetrically confined, with hole confinement being slightly stronger due to the associated heavier mass.

When the alloy disorder is introduced in the QW regions, the electron wave function is weakly affected and retains some characteristic of the envelope-type approximation. However the hole wave function exhibits a strong perturbation and is heavily confined in the QW region. This is expected because the Bi related resonance states are predicted to lie below the valence band edge of the GaAs material and strongly interact with the valence band through band-anticrossing interaction [11, 36]. Therefore the effect of Bi pairs and clusters will strongly modify the hole energies and the confinement of hole states.

S6. Charge densities for ordered double quantum well structures

Charge density plots for the triple and quadruple QW structures with ordered distribution of Bi atoms in the QW regions are shown in Fig. 2 of the main text. Here we show the same plots for double QW structures. Overall the character of the electron and hole ground states is consistent with what we expect from strongly coupled MQWs. At small values of QW separation, the two QWs are strongly coupled and therefore the electron and hole states form hybridized molecular states. For large separation, the coupling between the QWs becomes weak and therefore the electron and hole states tend to confine in individual QW regions. We find that coupling vanishes much quickly for the holes states and at $d=16$ nm, the ground hole state is nearly entirely confined

in a single QW region. On the other hand, the electron state is still weakly coupled even at 16 nm and turn into a completely decoupled state at about 24 nm separation.

S7. Charge densities for disordered MQW structures

The confinement of electron and hole wave functions in disordered MQW structures is strongly modified by the presence Bi pairs and clusters. Therefore it is expected that the charge density plots will exhibit drastically different confinements as a function of fluctuations in Bi positions. To demonstrate this effect, in this section we have considered three different random configuration of Bi atoms for each MQW structure and plotted the corresponding electron and hole charge densities as a function of the distance along the (001) axis. The random Bi configurations are labelled by R_1 , R_2 , and R_3 . Figs. S5, S6, and S7 show plots for MQW structures with $n=2$, 3, and 4, respectively. The charge density plots clearly show the strength and nature of alloy disorder effects on the character of electron and hole states in MQW devices. Overall we deduce the following important insights which are expected to be critical to understand future experimental measurements:

- 1) The inter-well coupling effect is completely vanished for the hole states, which are strongly confined in only one QW region for all values of n and d . Furthermore, the selection of a particular QW region for hole confinement is entirely arbitrary and is dependent on strength of disorder for that particular QW region.
- 2) The electron states still exhibit inter-well coupling effects but this effect is significantly weakened by the disorder. For
- 3) From the ordered MQW structures, we have found that the inter-well coupling for electron states vanishes for $d=24$ nm. However due to disorder related weakening of coupling, typically at 16 nm separation we find that the electron states are confined in individual QW regions and therefore exhibit no coupling effect.

S8. Interplay between alloy disorder and geometry parameters

In the main text of the paper, we have investigated the role of alloy disorder in the presence of small fluctuations in Bi composition x and width of QW w for a three quantum well structure with 4 nm separation between the QW regions. In this section, we study a second case where similar changes in x and w are introduced for a four QW structure with 4 nm separation between the QWs.

Let us first investigate the effect of Bi composition. Fig. S7 (a) shows the plot of electron and hole charge densities for reference case when all the four QWs have same 3.125% of Bi atoms. The alloy disorder dictates the confinement of hole state in the upper most QW region where as the electron state is weakly hybridized and mainly present in the upper two QWs. To check the extreme case, we increase the Bi composition of the lowest QW region in (b) and (c). The increased Bi composition of the lowest QW means it should now host the electron and hole states. However our calculations indicate that the hole state remains confined in the upper most QW region thus implying a strong alloy disorder effect which overcomes the Bi composition effect. The electron state however is slightly shifted towards the lower QW region as it experiences weaker impact from the alloy disorder.

In Figs. S7 (d-f), we investigate the effect of QW width variations. In part (e), we plot the reference case where all of the four QWs have uniform (8 nm) widths. When the width of a QW region is decreased (increased), the electron and hole states should move out (inside) that QW region. However in part (d), the hole state is moved inside the lowest QW region despite its smaller width of 7 nm. This is because the smaller width of QW would lead to a larger number of Bi pairs and clusters thus increasing the strength of alloy disorder which in spite of QW width induced energy shift confines the hole state in smaller width QW. On the other hand, when the lowest QW width is increased to 9 nm (in part f), the hole state is still confined in the uppermost QW region and the small change in hole energy is not sufficient to overcome the larger change from the alloy disorder. Overall these results clearly show that the alloy disorder is dominant over the ± 1 nm fluctuations in the QW width.

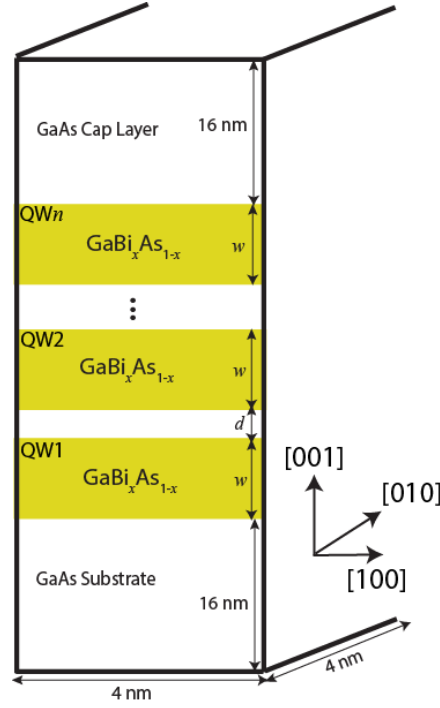


FIG. S1. Schematic diagram of a $\text{GaBi}_x\text{As}_{1-x}/\text{GaAs}$ multi-quantum-well structure is illustrated. The device consists of n number of QWs with d nm separation between the QWs and the width of each QWs is w nm. The thickness of both GaAs substrate and capping layer is 16 nm, and the lateral dimensions are 4 nm in each (100) and (010) directions. The boundary conditions are periodic in all three spatial dimensions.

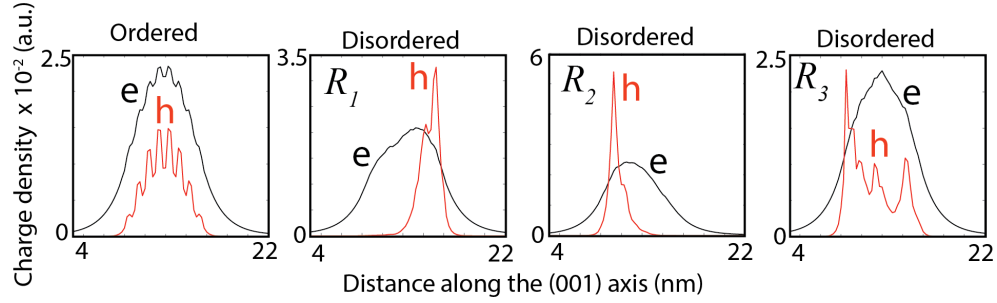


FIG. S2. Plots of the lowest electron (e) and the highest hole (h) charge densities ($|\Psi|^2$) are shown for single QW devices and for both ordered and disordered placement of Bi atoms. To highlight the impact of disorder, we plot three different random placements of Bi atoms (R_1, R_2, R_3). The electron states are weakly perturbed by disorder, whereas the hole states are high confined and clearly show significant impact from Bi pairs and clustering.

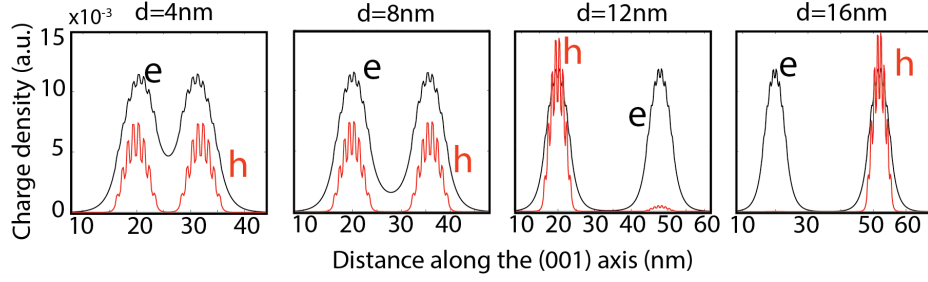


FIG. S3. Plots of the lowest electron (e) and the highest hole (h) charge densities ($|\Psi|^2$) are shown as a function of distance along the (001) axis are shown for a few selected separations d for double QW structures. For small separations between the QWs, strong effect of coupling leads to bonding-like hybridized states spread over all the QWs as well as on the GaAs spacer in-between them. For large separations, the coupling effect becomes weak for electron states and completely vanishes for the hole states.

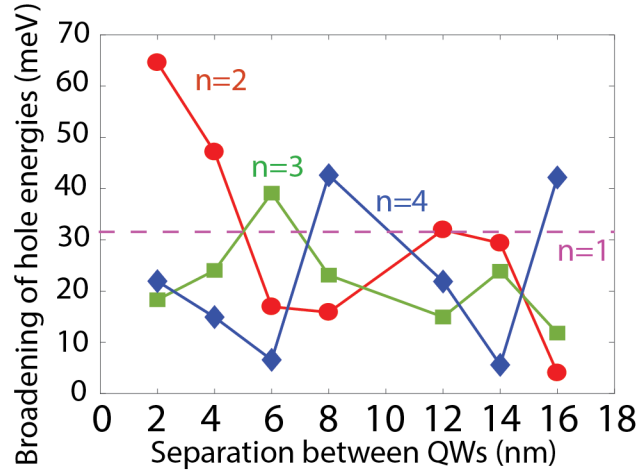


FIG. S4. Broadening of the highest hole energy levels is plotted for various QW devices ($n=1, 2, 3$, and 4) as a function of separation d between the QWs. The broadening is computed from the difference between minimum and maximum of hole energies computed from five different random placement of Bi atoms in the QW regions.

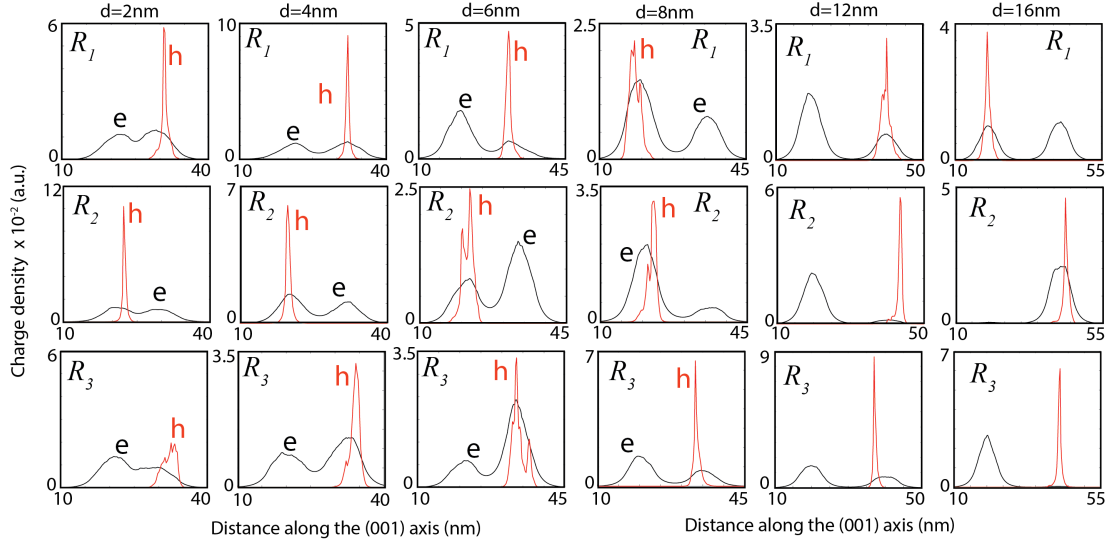


FIG. S5. Plots of the lowest electron (e) and the highest hole (h) state charge distributions ($|\Psi|^2$) are shown for double QW structures ($n=2$) as a function of the distance along the (001) axis for various QW separations (d). For each device, we plot three random distributions (R_1, R_2, R_3) of Bi atoms to show the character of alloy disorder on electron and hole states.

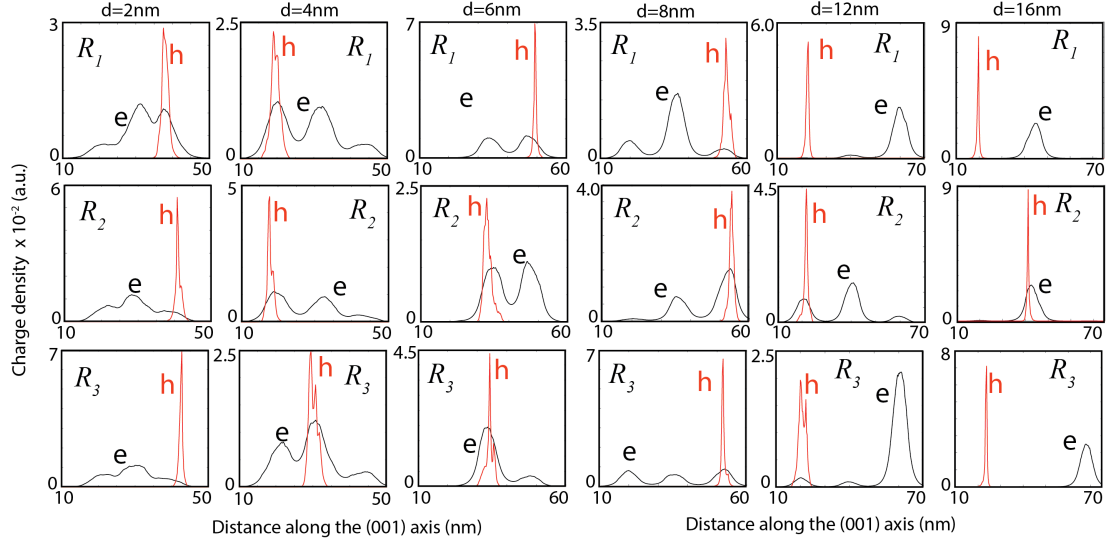


FIG. S6. Plots of the lowest electron (e) and the highest hole (h) state charge distributions ($|\Psi|^2$) are shown for three QW structures ($n=3$) as a function of the distance along the (001) axis for various QW separations (d). For each device, we plot three random distributions (R_1, R_2, R_3) of Bi atoms to show the character of alloy disorder on electron and hole states.

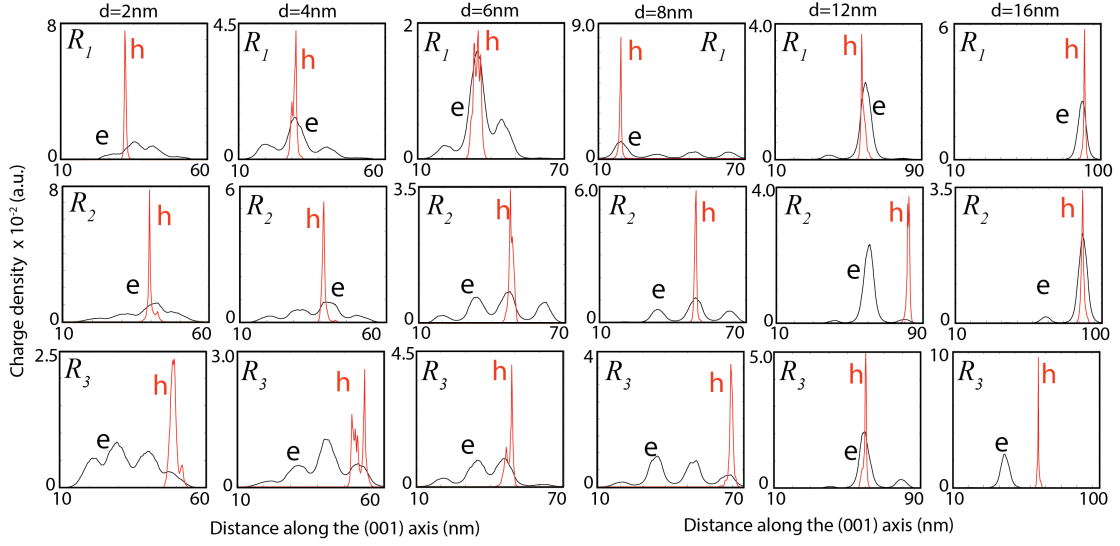


FIG. S7. Plots of the lowest electron (e) and the highest hole (h) state charge distributions ($|\Psi|^2$) are shown for four QW structures ($n=4$) as a function of the distance along the (001) axis for various QW separations (d). For each device, we plot three random distributions (R_1, R_2, R_3) of Bi atoms to show the character of alloy disorder on electron and hole states.

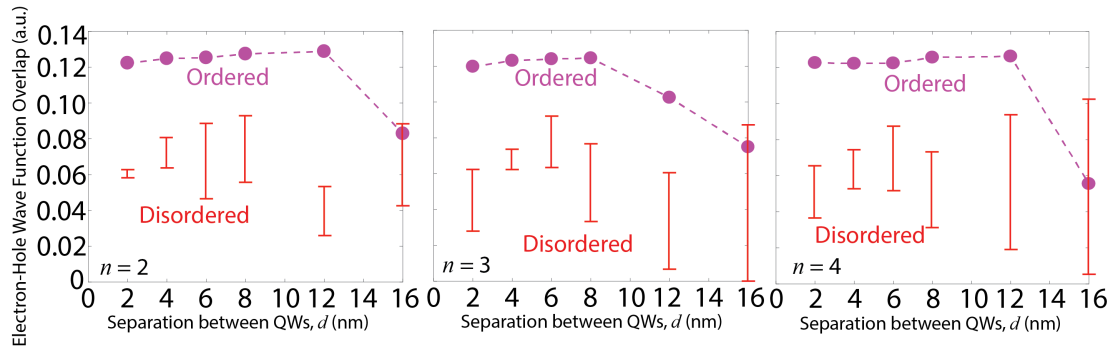


FIG. S8. Plots of overlap between the lowest electron and the highest hole wave functions are shown for both ordered and disordered QW structures, and for $n=2, 3$, and 4 .

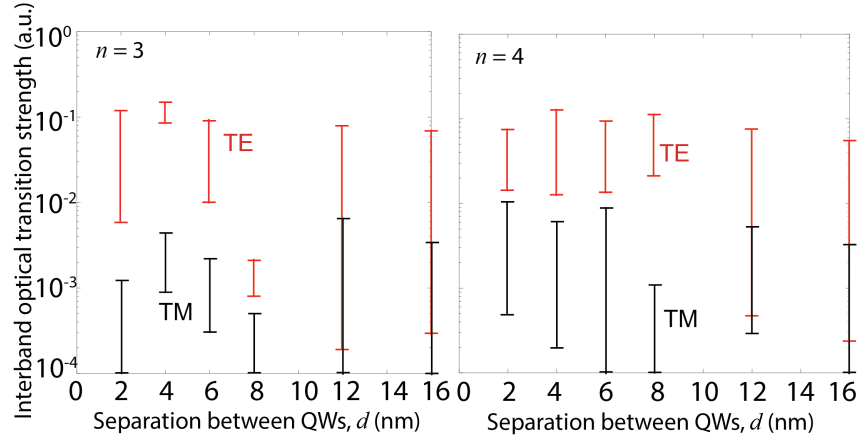


FIG. S9. Polarisation-resolved TE and TM inter-band optical transition strengths are plotted as a function of QW separations for triple and four QW structures.

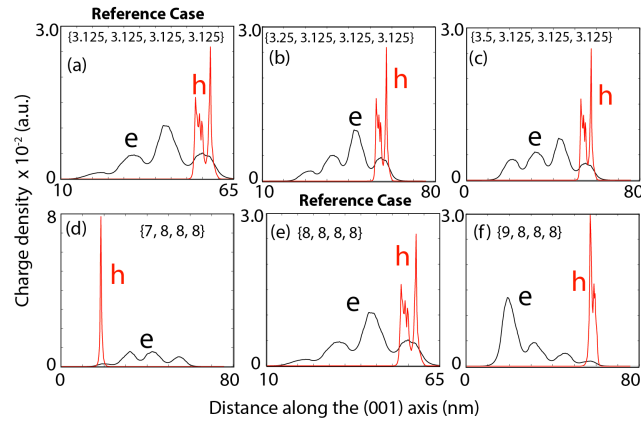


FIG. S10. (a-c) The Bi fraction of a four QW device ($n=4$) is varied as indicated by the labels $\{x_1, x_2, x_3, x_4\}$, where x_1, x_2, x_3 and x_4 are the Bi fractions of the lowest to the topmost QW regions, respectively. The widths w of all QWs are 8 nm and the separation between the QWs is 4 nm. (d-f) The width of the lowest QW in a four QW structure ($n=4$) is varied as indicated by the labels $\{w_1, w_2, w_3, w_4\}$, where w_1, w_2, w_3 , and w_4 are the widths of the QWs from the lowest to the topmost, respectively. The Bi fraction x of all QWs is 3.125% and the separation between the QWs is 4 nm.

* usman@alumni.purdue.edu

- [1] X. Wu *et al.*, ACS Photonics **4**, 1322 (2017).
- [2] I. P. Marko, C. A. Broderick, S. R. Jin, P. Ludewig, W. Stolz, K. Volz, J. M. Rorison, E. P. O'Reilly, and S. J. Sweeney, Sci. Rep. **6**, 28863 (2016).
- [3] P. Ludewig, N. Knaub, N. Hossain, S. Reinhard, L. Natterman, I. P. Marko, S. R. Jin, K. Hild, S. Chatterjee, W. Stolz, S. J. Sweeney, and K. Volz, Appl. Phys. Lett. **102**, 242115 (2013).
- [4] H. Li and Z. Wang, eds., *Bismuth-Containing Compounds* (Springer-Verlag New York, 2013).
- [5] R. D. Richards *et al.*, Solar Energy Materials and Solar Cells **172**, 238 (2017).
- [6] H. Kim *et al.*, J. of Cryst. Growth **452**, 276 (2016).
- [7] A. Johnson, Patent no. US 20140326301A1 (filed: August 14, 2012, issued: July 24, 2014).
- [8] B. Fluegel, S. Francoeur, A. Mascarenhas, S. Tixier, E. C. Young, and T. Tiedje, Phys. Rev. Lett. **97**, 067205 (2006).
- [9] P. Dongmo, Y. Zhong, P. Attia, C. Bomberger, R. Cheaito, J. F. Ihlefeld, P. E. Hopkins, and J. M. O. Zide, J. Appl. Phys. **112**, 093710 (2012).
- [10] Z. Batool, K. Hild, T. J. C. Hosea, X. Lu, T. Tiedje, and S. J. Sweeney, J. Appl. Phys. **111**, 113108 (2012).
- [11] M. Usman, C. A. Broderick, A. Lindsay, and E. P. O'Reilly, Phys. Rev. B **84**, 245202 (2011).
- [12] M. Usman, C. A. Broderick, Z. Batool, K. Hild, T. J. C. Hosea, S. J. Sweeney, and E. P. O'Reilly, Phys. Rev. B **87**, 115104 (2013).
- [13] C. A. Broderick, M. Usman, and E. P. O'Reilly, Semicond. Sci. Technol. **28**, 125025 (2013).
- [14] R. D. Richards, F. Bastiman, J. S. Roberts, R. Beanland, D. Walker, and J. P. R. David, J. Cryst. Growth **425**, 237 (2015).
- [15] M. A. G. Balanta, V. O. Gordo, A. R. H. Carvalho, J. Puustinen, H. M. Alghamdi, M. Henini, H. V. A. Galeti, M. Guina, and Y. G. Gobato, J. of Luminescence **182**, 49 (2017).
- [16] Y. I. Mazur *et al.*, J. of Luminescence **188**, 209 (2017).
- [17] M. Aziz *et al.*, J. of Luminescence **111**, 102102 (2017).
- [18] H. Makhoulfi *et al.*, Nanoscale Research Lett. **9**, 123 (2014).
- [19] M. A. G. Balanta *et al.*, J. Phys. D: Appl. Phys. **49**, 355104 (2016).
- [20] P. K. Patil *et al.*, Nanotechnology **28**, 105702 (2017).

- [21] M. Usman and E. P. O'Reilly, Appl. Phys. Lett. **104**, 071103 (2014).
- [22] C. A. Broderick, P. E. Harnedy, P. Ludewig, Z. L. Bushell, K. Volz, R. J. Manning, and E. P. O'Reilly, Semicond. Sci. Technol. **30**, 094009 (2015).
- [23] M. P. Polak *et al.*, Semicond. Sci. Technol. **30**, 094001 (2015).
- [24] L. C. Bannow *et al.*, arXiv:1709.09983v1 (2017).
- [25] P. N. Keating, Phys. Rev. **145**, 637 (1966).
- [26] M. Usman, T. Inoue, Y. Harda, G. Klimeck, and T. Kita, Phys. Rev. B **84**, 115321 (2011).
- [27] C. Gogineni *et al.*, Appl. Phys. Lett. **103**, 041110 (2013).
- [28] D. F. Reyes *et al.*, Appl. Phys. Express **6**, 042103 (2013).
- [29] C. R. Hall *et al.*, New J. Phys. **15**, 045028 (2013).
- [30] O. L. Lazarenkova, P. von Allmen, F. Oyafuso, S. Lee, and G. Klimeck, Appl. Phys. Lett. **85**, 4193 (2004).
- [31] P. R. C. Kent and A. Zunger, Phys. Rev. B **64**, 115208 (2001).
- [32] G. Klimeck, S. S. Ahmed, H. Bae, N. Kharche, R. Rahman, S. Clark, B. Haley, S. Lee, M. Naumov, H. Ryu, F. Saied, M. Prada, M. Korkusinski, and T. Boykin, IEEE Trans. Electron. Dev. **54**, 2079 (2007).
- [33] G. Klimeck, S. S. Ahmed, N. Kharche, M. Korkusinski, M. Usman, M. Prada, and T. Boykin, IEEE Trans. Electron. Dev. **54**, 2090 (2007).
- [34] M. Usman *et al.*, Nature Nanotechnology **11**, 763 (2016).
- [35] M. Usman, V. Tasco, M. Todaro, M. Giorgi, E. O'Reilly, G. Klimeck, and A. Passaseo, Nanotechnology **23**, 165202 (2012).
- [36] C. A. Broderick, M. Usman, S. J. Sweeney, and E. P. O'Reilly, Semicond. Sci. Technol. **27**, 094011 (2012).